Eur. Phys. J. A **16**, 55–61 (2003)
DOI 10.1140/epja/i2002-10069-9

THE EUROPEAN PHYSICAL JOURNAL A

New region of deformation in the neutron-rich $^{60}_{24}Cr_{36}$ and $^{62}_{24}Cr_{38}$

O. Sorlin[1,a], C. Donzaud[1], F. Nowacki[2], J.C. Angélique[3], F. Azaiez[1], C. Bourgeois[1], V. Chiste[1], Z. Dlouhy[4], S. Grévy[3], D. Guillemaud-Mueller[1], F. Ibrahim[1], K.-L Kratz[5], M. Lewitowicz[6], S.M. Lukyanov[7], J. Mrasek[4], Yu.-E. Penionzhkevich[7], F. de Oliveira Santos[6], B. Pfeiffer[5], F. Pougheon[1], A. Poves[8], M.G. Saint-Laurent[6], and M. Stanoiu[6]

[1] Institut de Physique Nucléaire, IN2P3-CNRS, F-91406 Orsay Cedex, France
[2] IReS, IN2P3-CNRS, Université Louis Pasteur, BP 28, F-67037 Strasbourg Cedex, France
[3] LPC, ISMRA, F-14050 Caen Cedex, France
[4] Nuclear Physics Institute, AS CR, CZ 25068, Rez, Czech Republic
[5] Institut für Kernchemie, Universität Mainz, D-55128 Mainz, Germany
[6] GANIL, B. P. 5027, F-14076 Caen Cedex, France
[7] FLNR, JINR, 141980 Dubna, Moscow region, Russia
[8] Departamento de Fisica Teorica, Universidad Autónoma de Madrid, Cantoblanco, 28049 Madrid, Spain

Received: 13 June 2002 /
Published online: 17 January 2003 –
Communicated by D. Guerreau

Abstract. The neutron-rich nuclei $^{60\text{-}63}_{23}V$ have been produced at GANIL via interactions of a 61.8 A · MeV ^{76}Ge beam with a ^{58}Ni target. Beta-decay to $^{60\text{-}63}_{24}Cr$ has been investigated using combined β- and γ-ray spectroscopy. Half-lives of the $^{60-63}V$ nuclei have been determined, and the existence of a beta-decay isomer in the ^{60}V nucleus is strongly supported. The observation of low-energy 2^+ states in ^{60}Cr (646 keV) and ^{62}Cr (446 keV) suggests that these isotopes are strongly deformed with $\beta_2 \sim 0.3$. This is confirmed by shell model calculations which show the dominant influence of the intruder g and d orbitals to obtain low 2^+ energies in the neutron-rich Cr isotopes.

PACS. 27.50.+e $59 \leq A \leq 89$ – 23.40.-s Beta decay; double beta decay; electron and muon capture – 21.60.Cs Shell model – 21.60.-n Nuclear-structure models and methods

1 Introduction

The $N = 40$ sub-shell closure is originally the $N_{\text{osc}} = 4$ harmonic-oscillator (HO) shell closure. However, the spin-orbit force in atomic nuclei splits the g ($l = 4$) orbital into two, the aligned configuration $g_{9/2}$ ($l + s$) is lowered and the anti-aligned $g_{7/2}$ is raised in energy. The $g_{9/2}$ orbital becomes an intruder state with respect to the $N_{\text{osc}} = 3$ HO shell and $N = 40$ is not any more a major shell closure. The relative importance of the single-particle gaps at 40 and 50 depends in both the strength of the spin-orbit interaction and the neutron-proton interaction. The strength of the sub-shell *closure* at $N = 40$ is characterized by the size of the gap between $f_{5/2}p_{1/2}$ and $g_{9/2}$ and by the possibilities to generate excitations across it.

The study of neutron-rich nuclei below $^{68}_{28}Ni_{40}$ is of special interest since many fascinating physics aspects are involved to model the evolution of the sub-shell closure at $N = 40$. The valence orbital $g_{9/2}$ is extremely important since it governs the properties of the neutron-rich $N \sim 40$ nuclei. Its effects are multiple, and act in favour or against an increase of a sub-shell closure. The two arguments in favor of a sub-shell closure are as follows.

A weakening of the spin-orbit surface term is predicted for very neutron-rich nuclei as their surface is expected to be more diffuse [1]. Consequently, the $g_{9/2}$ orbital would move closer to the next upper orbital, increasing the size of the $N = 40$ gap. In addition to this, the presence of this positive-parity orbital above fp negative-parity ones strongly hinder excitations which preserve parity symmetry. As a result, quadrupole excitations across the $N = 40$ gap are substancially reduced in $^{68}_{28}Ni_{40}$ [2].

However, pairing correlations between $f_{5/2}p_{1/2}$ and $g_{9/2}$ orbitals result in an apparent superfluidity of the nuclei, since neutrons are "attracted" by the presence of the $g_{9/2}$ valence orbital [2]. In addition to this, the two first sub-states of the $g_{9/2}$ orbital are steeply decreasing when the quadrupole deformation is increased. These two latter effects lead to an effective erosion of the sub-shell gap at $N = 40$.

[a] e-mail: sorlin@ipno.in2p3.fr

Hannawald *et al.* [3] have deduced that the neutron rich $^{66}_{26}\mathrm{Fe}_{40}$ is deformed with a quadrupole deformation $\beta_2 \sim 0.26$. This was deduced from the determination of the low energy of its first 2^+ excited state, $E(2^+) = 562.5$ keV. Since the $_{24}$Cr isotopes lie at mid proton $f_{7/2}$-shell, between $Z = 20$ and $Z = 28$, protons can additionally destabilize the nucleus and favor deformation. However, given all the competing effects mentioned above, reliable theoretical predictions are difficult to establish for the neutron-rich nuclei around $N = 40$.

The study of these neutron-rich nuclei at/around $N = 40$ sub-shell closure is also of astrophysical relevance. Recent astronomical observations of old stars in the galactic halo reveal the probable existence of a "weak" r-process component which would produce nuclei of masses below $A = 130$ from neutron-rich progenitors. This "weak" process could extend down to light masses, and be responsible for the observation of correlated isotopic anomalies in the neutron-rich ^{48}Ca-^{50}Ti-^{54}Cr-^{58}Fe-^{64}Ni-^{66}Zn in certain inclusions of meteorites. Therefore, the presence and strength of any shell or sub-shell effect at $N = 28$, $N = 32$ and $N = 40$ far-off stability is still actively researched.

Beta-decay studies provides the first tool which can be used for understanding the evolution of nuclear structure in the neutron-rich Cr isotopes. This paper focus on the beta-decay of $^{60\text{-}63}$V, aiming to deduce nuclear-structure information from their half-lives and from their main γ transitions.

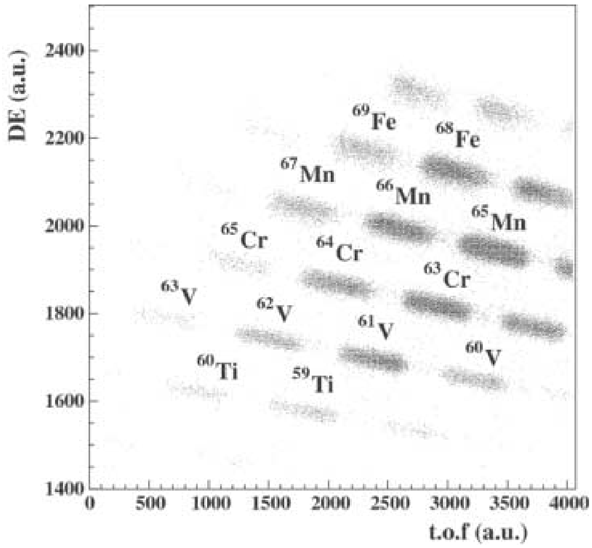

Fig. 1. Identification of the nuclei produced in the experiment by their energy loss (DE) and time of flight (t.o.f), given in arbitrary units.

2 Experimental procedure and results

The neutron-rich $^{60\text{-}63}_{23}$V isotopes have been produced at GANIL by the fragmentation of a 61.8 A · MeV $^{76}\mathrm{Ge}^{30+}$ beam, of mean intensity 1 eμA, onto a ^{58}Ni target of 118 μm thickness. The nuclei of interest were separated by the LISE3 achromatic spectrometer which was tuned to optimize the transmission rate of ^{62}V. A wedge-shaped Be foil of 221 μm thickness was placed in the intermediate focal plane of the spectrometer in order to reduce the rate of nuclei close to stability. As a consequence, the ^{60}V nuclei were partially eliminated. The nuclei transmitted through the spectrometer were identified by means of 3 consecutive 300, 300, 1500 μm silicon detectors. The first two served for the energy loss and time-of-flight measurements. The last one, into which the nuclei were implanted, determined their residual energies. It was divided in sixteen 3 mm wide, 46 mm height vertical strips. The rate of nuclei implanted was about ten per minute in each strip. Figure 1 shows an energy loss *versus* time-of-flight spectrum obtained for the nuclei transmitted in the experiment. The total number of ^{60}V, ^{61}V, ^{62}V and ^{63}V implanted was 1196, 5858, 1152 and 127, respectively. The production rates of ^{61,62}V nuclei have been increased for at least a factor of 10 by using a ^{76}Ge primary beam instead of ^{86}Kr [4], whose mass number is further away from that of the fragments of interest.

Each time a nucleus was implanted in one of the strips #i, the primary beam was switched off during 1 second to collect the beta-rays of its decay. These beta-rays were attributed to a precursor nucleus when detected in the same #i or adjacent #$i \pm 1$ strip. About 75% of the beta-rays were detected in the same strip as the precursor nucleus. Additional 20% were detected in the adjacent ones. They correspond to cases where the precursor nucleus was implanted at the boarder of two strips. In such cases, the path of a beta-particle in an adjacent strip was considerably longer and the detection efficiency was subsequently enhanced. Beta-decay time spectra correlated with the implantation of $^{60\text{-}63}$V are shown in fig. 2. The fitting procedure to determine the half-lives of $^{60\text{-}63}$V includes five parameters: the half-lives of the mother, the daughter and grand-daughter nuclei, the β-efficiency and the background rate over the 1 second collecting time. The half-lives of daughter (Cr) and grand-daughter nuclei (Mn) have been taken from refs. [4] and [3]. The β-efficiency has been found to be very similar for all nuclei, $\epsilon_\beta \simeq 90(5)\%$, though they were not centered at the same horizontal position in the strips. This efficiency has been increased by a factor of five as compared to ref. [4] by using a thicker implantation Si-detector (1500 μm instead of 500 μm) and a high pre-amplification gain dedicated to the collection of low-energy signals of β-rays. The beta background was due to the decay of long-lived nuclei produced by filiations. With a better production rate of the nuclei and an increase of the beta-efficiency, the half-lives of ^{61}V and ^{62}V have been obtained with better accuracy: $T_{1/2} = 47 \pm 1.2$ ms (old value 43 ± 7 ms [4]) and $T_{1/2} = 33.5 \pm 2$ ms (old value 65 ± 31 ms [4]), respectively. The half life of the $N = 40$ nucleus ^{63}V, $T_{1/2} = 17 \pm 3$ ms, is determined for the first time. The half-life of ^{60}V, 68 ± 4.5 ms, is shorter than that of 122 ± 18 ms determined in ref. [4]. This surprising feature will be discussed below.

Four Ge detectors were placed around the implantation detector for the detection of the main γ-transitions

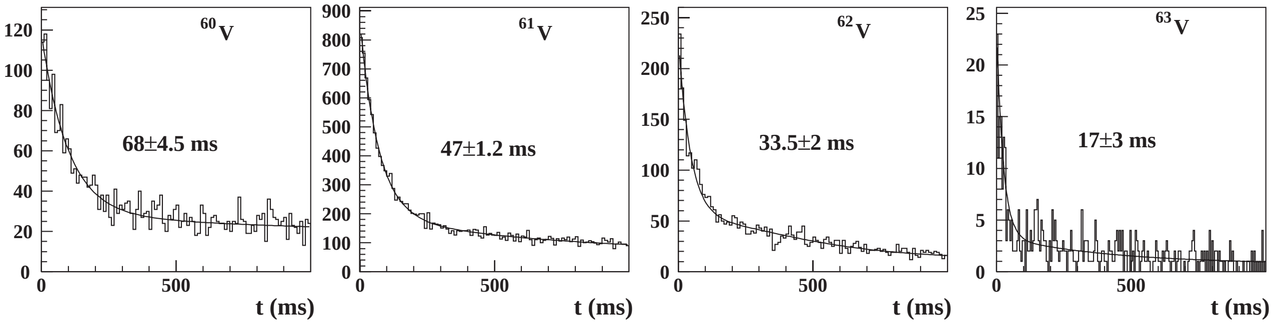

Fig. 2. Beta-decay curves of $^{60\text{-}63}$V. The corresponding half-lives $T_{1/2}$ are included for each isotope. The beta-decay curve of ^{60}V may contain two beta-decaying components, with one from a β-isomer.

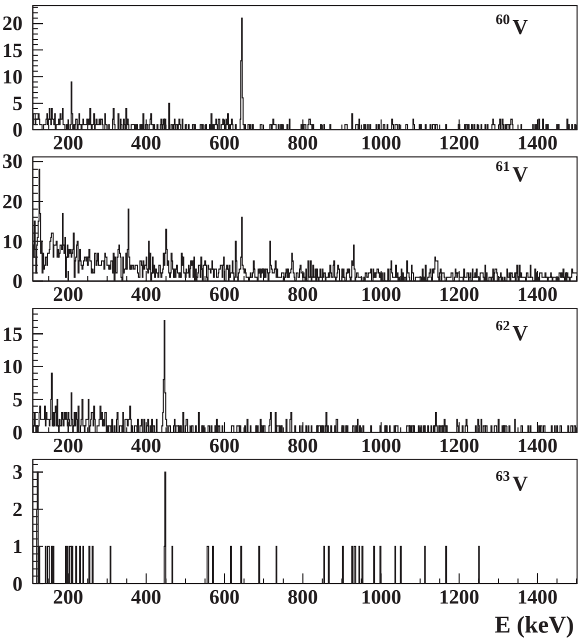

Fig. 3. Beta-gated γ-ray spectra following the decay of $^{60\text{-}63}$V (from top to bottom). γ-events are taken within a 300 ms time-window following the β-emission to eliminate against the rate of photons emitted by the daughter nuclei. The intense γ-rays at 646 keV (^{60}V) and 446 keV (^{62}V) are assigned as the $2^+ \to 0^+$ transitions in ^{60}Cr and ^{62}Cr, respectively.

following β-decay. The beta-gated γ-efficiency $\epsilon_{\beta\gamma}$ has been determined using an additional setting of the spectrometer optimized for the production of ^{67}Co and ^{69}Ni whose γ-branchings are known from ref. [5] and from refs. [6,7], respectively. About 9% of ^{69}Ni is produced in its $1/2^-$ beta-decay isomer, which decays in 74(9)% of all cases through the 1298 keV γ-ray [8,9]. After having corrected for this abundance of ^{69m}Ni, a consistent γ-efficiency has been extracted from the lines at 679 keV and 695 keV in ^{69}Ni and ^{67}Co, respectively. This results in $\epsilon_{\beta\gamma} = 6.5 \pm 1.3\%$ at about 680 keV. The determination of the γ-efficiency has been obtained independently using a ^{152}Eu source located at the Si-strip detector position. We have obtained a value of ϵ_γ similar to that of $\epsilon_{\beta\gamma}$, which confirms that the β-efficiency was close to 100%.

Beta-delayed gamma-ray spectra of ^{60}V and ^{62}V (fig. 3) exhibit γ-lines at 646(1) keV and 446(1) keV, respectively. The ratio of γ's in the peaks with respect to the number of implanted nuclei is 56(14)% and 37(9)%, respectively. Given the total number of photons in the peaks and the evolution of ϵ_γ as a function of the energy ($\epsilon_\gamma = 2.7(3)\%$ at 2 MeV), it is clear that no other peak with similar intensity is present in the spectra within the first 2 MeV. Since the strongest transition observed in the beta-decay of odd-odd to even-even nuclei is usually the $2^+ \to 0^+$ transition, it is assumed that the 2^+ energies of ^{60}Cr and ^{62}Cr nuclei are 646 keV and 446 keV, respectively.

It is interesting to note that the two γ-lines at 646(1) keV and 446(1) keV are also observed in the β-gated γ spectra of ^{61}V (about 22 counts) and ^{63}V (about 4 counts), respectively. This means that the 2^+ excited states of ^{60}Cr and ^{62}Cr are fed through the β-delayed neutron decay of ^{61}V and ^{63}V. From the intensity of the $2^+ \to 0^+$ transition, we can deduce lower limits of the β-delayed neutron branching P_n of $\sim 6\%$ for ^{61}V and of $\sim 35\%$ for ^{63}V. We give a lower limit of the P_n, since it is deduced from the β delayed-neutron branching decay through the known $2^+ \to 0^+$ γ-transition only.

3 Discussion

Information on the structure of V and Cr in this mass region can be extracted from the measurement of their half-lives and from the determination of the 2^+ energies of even-even nuclei. These two properties are examined in the following.

3.1 Beta-decay isomer in ^{60}V

The present half-life of ^{60}V differs significantly from that obtained in ref. [4]. Similar discrepancy between the two experiments are not seen in any other nucleus measured in common. Since the γ-line at 646 keV is seen in both experiments, it is sure that the same nucleus has been studied. It is, therefore, probable that a β-isomer is present in ^{60}V. This would happen if a high-spin difference existed between the ground state and an excited state, close in energy. The half-life obtained in each experiment depends on the relative production of the isomer in the fragmentation reaction. One of these beta-decaying states would have a short half-life (68 ms or less), the other one would be longer (122 ms or more). It is important to remind that the two experiments did not use the same projectile to produce the fragments of interest. This could explain why either a low- or high-spin state is favored. This presence of an isomer in ^{60}V is reinforced by the existence of a similar configuration in the isotone $^{62}_{25}$Mn$_{37}$. The high-spin state, corresponding to a 671 ms half-life, has been found by Hannawald *et al.* [3] from the study of the β-neutron decay of ^{62}Mn. This confirmed the first measurement of Runte *et al.* [10]. The low-spin isomer, with a half-life of about 90 ms, has been first evidenced from the decay of the mother nucleus of ^{62}Mn [4], *i.e.* $^{62}_{24}$Cr. Beta-decay selection rules imply that the even-even ^{62}Cr, with spin 0^+, favors low spins in its decay. The high-spin β-isomer was therefore not fed in the β-decay of ^{62}Cr. It is seen from this example that the β-decay of even-even nuclei may act as a "filter" for selecting the low-spin states. Consequently, we have looked at the beta-decay of the even-even mother nucleus ^{60}Ti in order to select the low-spin beta-decaying state in ^{60}V. A good fit of the decay curve of ^{60}Ti is obtained when using a short daughter half-life for ^{60}V of $T_{1/2} = 40(15)$ ms. This is in accordance with the present direct determination of the ^{60}V half-life (68 ± 4.5 ms), though a bit shorter. Therefore, the ^{60}V beam might contain a small fraction of a long-lived beta-decaying state in the present experiment. In the following, we adopt a half-life of 40(15) ms, which corresponds to the β-decay of one state in ^{60}V.

For ^{60}V, the Finite Range Droplet Model [11] predicts that the potential-energy surface is very soft with two shallow minima at different shapes. $^{60}_{23}$V$_{37}$ is predicted to be oblate ($\beta_2 = -0.11$) in its ground state, the prolate minimum ($\beta_2 = +0.11$) being 115 keV higher in energy. For oblate shapes, the downsloping $g_{9/2}$ intruder orbital $[404]9/2^+$ can be occupied by neutrons. The presence of this orbital close to the ground state has been evidenced in the neighboring nucleus $^{59}_{24}$Cr$_{35}$ which exhibits a $9/2^+$ state at 503 keV. It is, therefore, possible that the 37th neutron occupies the intruder configuration in its ground state or in a nearby one. This neutron would couple with a $[303]5/2^-$ proton in ^{60}V to yield negative-parity states of spins J ranging from 2 to 7. With the prolate configuration, the expected spins are lower, from $J = 1$ to 4, and of positive parity. Following these assumptions, many levels should be found close in energy in ^{60}V with possibly large spin differences. Two gamma-decaying isomers of 13(3) ns and 320(90) ns half-lives have already been evidenced in ^{60}V by J. M. Daugas [12].

3.2 QRPA calculations for the β-decay of ^{60,62}V

We have used the QRPA model of Möller and Randrup [13] to calculate Gamow-Teller (GT) strength functions and β-decay half-lives $T_{1/2}$ of ^{60}V and ^{62}V as a function of their deformation. The Q_β-values used are taken from mass measurements in the case of ^{60}V [14] and from the predictions of Möller *et al.* [11] for the neutron-rich ^{62}V. Deformation-dependent wave functions and single-particles energies are obtained with the Folded-Yukawa potential. In the beta-decay, the GT strength can be shared among excited states and the ground state of the daughter nucleus according to the beta-decay selection rules. These excited states can subsequently decay or not through the first 2^+ state of ^{60}Cr and ^{62}Cr. The relatively low feeding of the first 2^+ state (P_{2^+}) indicates that the decays of ^{60}V (56(14)%) and ^{62}V (37(9)%) partly occur directly to the g.s. of the daughter nuclei or/and to levels which bypass the 2^+ state.

The variation of $T_{1/2}$ of ^{60}V as a function of the deformation parameter β_2 is $(T_{1/2}\,(\mathrm{ms}), \beta_2) = (55, -0.257)$, (18, −0.20), (16, −0.137), (45, 0.183), (36, 0.257), (38, 0.275). From these deformation-dependent calculations, it seems that the short beta-decay component, $T_{1/2} = 40(15)$ ms, can be obtained with whatever deformation parameter β_2 considered. The measured half-life alone, therefore, does not provide a sensitive means to constrain the deformation parameter. The calculated probability of feeding the ground state ($P_{\mathrm{g.s.}}$) in the daughter nucleus is higher than 5% only for deformation parameters of $\beta_2 \simeq -0.20$ ($P_{\mathrm{g.s.}} = 45\%$) and $\beta_2 \simeq +0.25$ ($P_{\mathrm{g.s.}} = 12\%$). The relatively low experimental value P_{2^+} could be explained, in the case of $\beta_2 \simeq -0.20$, by the large value of $P_{\mathrm{g.s.}}$.

In the case of ^{62}V decay, the variation of $T_{1/2}$ as a function of deformation is very weak: $(T_{1/2}\,(\mathrm{ms}), \beta_2) = (19,$ $-0.33)$, (17, −0.275), (21, −0.11), (23, 0.0), (23, 0.11), (34, 0.22), (36, 0.275), (30, 0.33). Thus, the experimental half-life of $T_{1/2} = 33.5(2)$ ms is almost consistent with any calculated values and does not strongly favor any deformation parameter. A large value of g.s. feeding, $P_{\mathrm{g.s.}} = 35\%$, is found for a strongly oblate shape $\beta_2 \simeq -0.3$. For any other deformation parameter, the calculated $P_{\mathrm{g.s.}}$ does not exceed 10%. The low value of P_{2^+} could be due to a large $P_{\mathrm{g.s.}}$ and to a high delayed-neutron emission probability P_n. In such a case, the beta-decay of ^{62}V would be partly depleted to excited states in ^{61}Cr without feeding the $2^+ \to 0^+$ transition in ^{60}Cr. The calculated P_n of ^{62}V is about 20–30% for $-0.11 < \beta_2 < 0.33$, and three times weaker for larger oblate deformation.

We should note that the decay of ^{60,62}V to ^{60,62}Cr may occur via mother-to-daughter shape transition. Current theoretical models cannot treat properly parent-daughter pairs with different deformations. As a consequence, the conclusions deduced above would be changed if such a shape transition occurs. It is very likely for the case of ^{60}V decay, since both the mother and daughter nuclei are predicted to have potential-energy surfaces with very shallow minima at different shapes.

3.3 The E(2^+) evolution towards N = 40

It is possible to extract deformation parameter β_2 for ^{60,62}Cr from the energy of their 2^+ states by using the

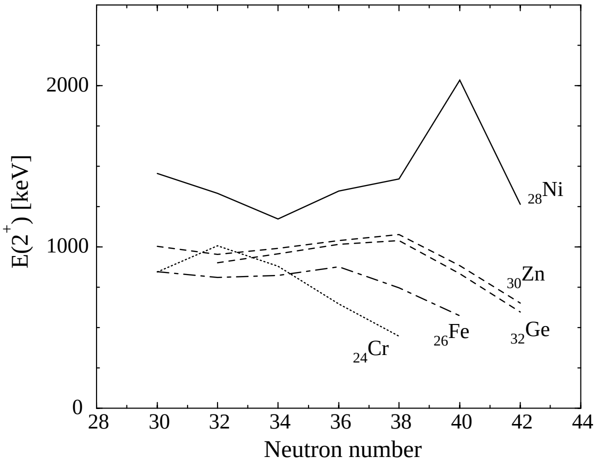

Fig. 4. 2^+ energies in the Ca, Cr, Fe and Ni isotopic chains around $N = 40$. Experimental values of ${}^{58}Cr$ and in the neutron-rich ${}^{64,66}Fe$ have been taken from refs. [17] and [3], respectively.

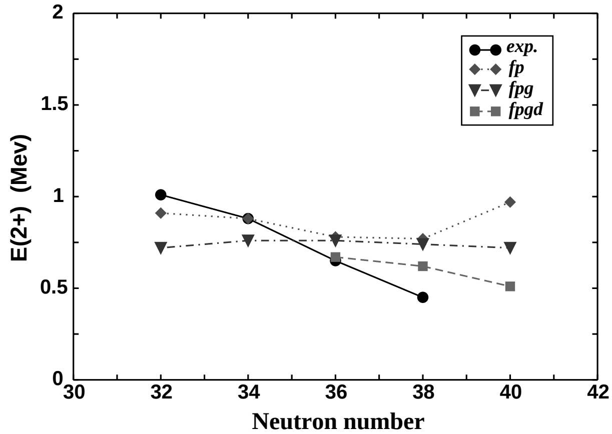

Fig. 5. Excitation energy of the 2^+ state for Cr isotopes (*pf*, *pfg* and *pfgd* calculations *versus* experimental values).

empirical formula of Raman *et al.* [15,16]:

$$\beta_2 = \text{const} \times \sqrt{A^{-0.69}/E(2^+)}. \tag{1}$$

A reference value for a nearby deformed nucleus can be taken from ${}^{76}Ge$ ($E(2^+) = 563\,\text{keV}$) in which a deformation parameter of $\beta_2 = 0.26$ has been extracted from the measurement of its $B(E2)$ [18]. The above equation then leads to $\beta_2 \simeq 0.27$ and $\beta_2 \simeq 0.31$ for ${}^{60}Cr$ and ${}^{62}Cr$, respectively. From this equation, oblate or prolate shapes cannot be distinguished. These deformations compare reasonably well with the predictions of FRDM [11] and ETFSI [19], for which prolate ground states of $\beta_2 \simeq +0.18$ and $\beta_2 \simeq +0.32$ are predicted for ${}^{60}Cr$ and ${}^{62}Cr$, respectively.

The $E(2^+)$ systematics of the even-even ${}_{24}Cr$, ${}_{26}Fe$, ${}_{28}Ni$, ${}_{30}Zn$ and ${}_{32}Ge$ are shown in fig. 4. The behavior of the $E(2^+)$, when approaching the $N = 40$ neutron number, is very different at $Z = 28$, $Z < 28$ and $Z > 28$. The tenuous effect of a spherical neutron sub-shell closure at $N = 40$, as evidenced in the proton-magic Ni isotopic chain by an increase of the 2^+ energy, is quickly washed out with the addition or removal of proton pairs. The behavior of the $Z > 28$ nuclei have been discussed already in ref. [20]. In the ${}_{30}Zn$ and ${}_{32}Ge$ isotopic chains, the spherical gap at $N = 40$ is comparable to the pairing energy difference between the fp states and the g intruder level [8,21,2]. This results in a high probability of scattering pairs of neutrons into the intruder g orbitals ($\nu[440]1/2^+$ and $\nu[431]3/2^+$), which are steeply downsloping as a function of prolate deformation. This leads to moderately deformed nuclei at $N = 40$. When removing protons from a Ni core, it is found that the decrease of the 2^+ energies is much steeper, emphasizing that the deformation is stronger in the Cr chain. This feature can be *qualitatively* understood for at least two reasons. As the ${}_{24}Cr$ isotopes reside at mid-occupancy of the $\pi f_{7/2}$-shell, the first two proton orbitals above $Z = 20$ have downsloping energies as deformation is increased. This favors a minimum of the potential-energy surfaces at large deformation. In addition, the strong proton-neutron interaction $\pi f_{7/2}\ \nu f_{5/2}$ can modify the size of the spherical sub-shell gap at $N = 40$. When protons are removed from the $\pi f_{7/2}$ orbital, the spin-orbit partner $\nu f_{5/2}$ is shifted to higher energies, thus coming closer to the intruder $g_{9/2}$ orbital. As a consequence, the ordering of levels are changed from ${}_{28}Ni$ to ${}_{20}Ca$ nuclei. In addition to the decrease of the $N = 40$ sub-shell gap, it provides an increase of neutron pair scattering from the $p_{1/2}$ to both the $f_{5/2}$ *and* $g_{9/2}$ orbitals [2]. The first experimental evidence of this monopole interaction $f_{7/2}f_{5/2}$ is the appearance of the $N = 32$ sub-shell closure. This was shown by Huck *et al.* [22] who have found an increase of 2^+ energy in ${}^{52}Ca_{32}$. This increase of 2^+ energy at $N = 32$ is also seen in the Cr chain, though with a somewhat weaker intensity (see fig. 4). This $N = 32$ sub-shell closure has been discussed extensively by Prisciandaro *et al.* who measured the 2^+ energy of ${}^{58}Cr$ [17]. This has also been discussed by Kanungo *et al.* [23] from the viewpoint of neutron-separation energy systematics. This sub-shell closure should be seen in the Ti chain, which lies between ${}_{20}Ca$ and ${}_{24}Cr$. Beta-decay of ${}^{54}Sc$ has been studied in ref. [24] to search for main γ-transitions in ${}^{54}_{22}Ti_{32}$. However, this experiment was not conclusive enough to firmly establish the energy of the 2^+ state in ${}^{54}Ti$.

In order to understand the origin of the onset of collectivity in the neutron-rich Cr isotopes, we have performed a series of shell model calculations, starting with their description within the *fp*-shell and progressively enlarging the valence space to include the higher shells $1g_{9/2}$ and $2d_{5/2}$. In the *fp* space, we use the recently defined KB3G version of the original Kuo-Brown G-matrix [25]. This interaction gives an excellent overall agreement with the spectroscopic data all over the fp-shell and can be considered as one reference interaction (among others like FPD6 [26]). In this space, the $N = 40$ sub-shell closure is effective. Figure 5 shows the evolution of the 2^+ excitation energies, as a function of the neutron number, compared to the experiment. Up to $N = 34$, the results of the *fp*-space calculation agree with the experiment. Beyond, they strongly diverge from the experimental trend as the cal-

Table 1. Calculated electromagnetic properties for ^{60,62,64}Cr in the *fpgd* space.

	^{60}Cr	^{62}Cr	^{64}Cr
$E^*(2^+)$ (MeV)	0.67	0.65	0.51
Q_s(e·fm^2)	−23	−27	−31
$BE2\downarrow$(e^2·fm^4)	288	302	318
Q_i(e·fm^2) from Q_s	82	76	109
Q_i(e·fm^2) from $B(E2)$	101	103	106
$E^*(4^+)$ (MeV)	1.43	1.35	1.15
Q_s(e·fm^2)	−37	−30	−43
$BE2\downarrow$(e^2·fm^4)	426	428	471
Q_i(e·fm^2) from Q_s	102	84	119
Q_i(e·fm^2) from $B(E2)$	117	117	123

culated 2^+ energies remain constant up to $N = 38$ and increase at ^{64}Cr$_{40}$, while experimentally they decrease. These discrepancies indicate that $N = 40$ cannot be considered as a good shell closure in the neutron-rich Cr isotopes.

As already noticed in the case of ^{68}Ni$_{40}$, the neutron $1g_{9/2}$ orbital plays a major role at $N = 40$ because of the strong cross-shell pairing correlations. This effect is responsible, at $N = 40$, for a strong population of this latter orbital, giving to ^{68}Ni a mixed character of semi-magic and superfluid nucleus [2]. Therefore, as a second step, we adopt the valence space and the effective interaction employed in [2], denoted by *fpg*. This valence space consists of a ^{48}Ca core (more precisely, a ^{40}Ca core with eight $f_{7/2}$ frozen neutrons), the $f_{7/2}$ $p_{3/2}$ $p_{1/2}$ and $f_{5/2}$ active orbitals for protons and the $p_{3/2}$ $p_{1/2}$ $f_{5/2}$ and $g_{9/2}$ active orbitals for neutrons. The calculations in this valence space describe well the behaviour of the 2^+ energies and $B(E2)$'s for the Ni isotopes ranging from $N = 28$ to $N = 40$. In addition, we have checked that the *fpg* description is still valid for the Cr chain at $N = 35$. For this purpose, we have verified that we can reproduce the experimental low-energy states in ^{59}Cr [4] and the $9/2^+$ isomer at 503 keV [27]. The *fpg* calculation predicts the $9/2^+$ isomer at 470 keV, which is in good agreement. The results of the *pfg* calculation for the chromiums are shown in fig. 5. It is evident that this calculation is also unable to reproduce the steep decrease of the 2^+ excitation energy observed experimentally beyond $N = 36$. The very low excitation energy of the 2^+ state in ^{62}Cr, suggests a strong deformation, which cannot be obtained by the inclusion of the $1g_{9/2}$ orbit alone.

It was proposed by Zuker *et al.* [28] that the minimal valence spaces able to develop quadrupole collectivity should contain at least a $(j, j-2\ldots)$ sequence of orbits. For example, in the so-called "island of inversion" around $N = 20$, the role of the $2p_{3/2}$ orbital is essential and it has to be added to its quasi-$SU3$ counterpart —the $1f_{7/2}$ orbital— in order to reproduce the onset of deformation. Similarly, in the $N = 40$ region, the $1g_{9/2}$ orbital and its quasi-$SU3$ counterpart the $2d_{5/2}$ have to be taken into account simultaneously [29]. The resulting valence space is called *pfgd*. In the actual calculations we are forced to block partly the $2p_{3/2}$ neutron orbital, imposing a minimal occupancy of two neutrons, due to the large dimensionalities of the calculation. The effective interaction for the *gd* part of the new space is, as the one used before, from a realistic interaction derived by the Oslo group [30].

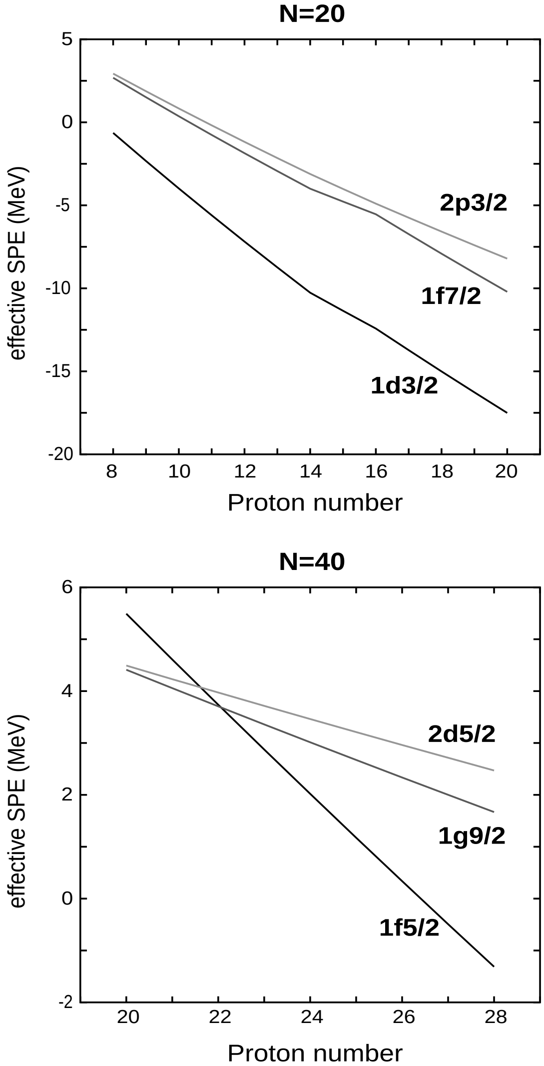

Fig. 6. Evolution of the neutron effective single-particle energies for the $N = 20$ isotones (top panel) and for the $N = 40$ isotones (bottom spectrum)

The inclusion of the $2d_{5/2}$ orbital increases the collectivity and decreases the 2^+ excitation energies, which become closer to the experimental values (fig. 5). In particular, the 2^+ excitation energy reaches its minimum value for ^{64}Cr, at the "would be" $N = 40$ neutron shell closure. In table 1, the $B(E2)$ values, the spectroscopic and the intrinsic quadrupole moments (Q_s and Q_i respectively), all obtained in the *pfgd* space, are shown for $^{60\text{-}64}$Cr. In the ^{64}Cr case, the 2^+ and 4^+ states have similar (and large) Q_i and Q_s values, a characteristic feature of an axial rotor. These quadrupole moments correspond to a deformation parameter $\beta_2 \sim 0.3$.

It is interesting to draw a parallel between the situations encountered in the $N = 20$ and $N = 40$ regions, which correspond to harmonic-oscillator shell closures $N_{osc} = 3$ and $N_{osc} = 4$, respectively. For this purpose, we show in fig. 6 the calculated neutron effective single-particle energies [31] in the two cases. For the top spectrum, which corresponds to the $N = 20$ region, the interaction of refs. [32,33] has been used, whereas the *pfgd* interaction is used in the bottom spectrum for the $N = 40$ region. In the so-called "island of inversion" at $N = 20$, the deformation develops at large neutron excess because two circumstances concur: First, the reduction of the $N = 20$ gap between the $d_{3/2}$ and the $f_{7/2}$ intruder state with increasing neutron excess, facilitates the excitation of neutrons across $N = 20$. This reduction is due to the proton-neutron interaction between the $\pi d_{5/2}$–$\nu d_{3/2}$ orbitals [31]. Second, the quasi-degeneracy between the $f_{7/2}$ and the $p_{3/2}$ orbits gives rise to a sequence of j, $j-2$ spins above the Fermi surface which favors deformed configurations of 2p-2h character that dominate the ground state. As a result, the nuclei lying next to spherical $^{34}_{14}Si$, $^{32}_{12}Mg$ and $^{30}_{10}Ne$, are deformed. Though the $N = 20$ shell gap is larger than the $N = 40$ one, the situation is similar if we replace the sequence of levels —$1d_{3/2}$, $1f_{7/2}$ and $2p_{3/2}$— in $N = 20$ by —$1f_{5/2}$, $1g_{9/2}$ and $2d_{5/2}$— in $N = 40$. The removal of protons from the $\pi 1f_{7/2}$ orbital in $^{68}_{28}Ni$ provokes a dramatic increase of the energy of the $\nu 1f_{5/2}$ orbital and a lowering of the $1d_{5/2}$ one, changing completely the ordering of these orbitals in the neutron-rich Ti and Ca isotopes. In Cr and Fe nuclei, the relevant $(j, j-2)$ levels are close to each other and nearby the Fermi surface. This provides ideal conditions for developing quadrupole deformation beneath $^{68}_{28}Ni$, *i.e.* for $^{66}_{26}Fe$ and $^{64}_{24}Cr$.

4 Conclusion

Beta-decay studies of neutron-rich $^{60\text{-}63}V$ has been achieved using combined β- and γ-ray spectroscopy. The half-lives of $^{60\text{-}63}V$ have been determined and compared to QRPA model predictions assuming various deformation parameters. The half-life of ^{60}V differs from previous measurement, which could be due to the presence of a β-decay isomer. The $N = 40$ nucleus ^{63}V is studied for the first time. The 2^+ energies of ^{60}Cr and ^{62}Cr have been found to be 646(1) and 446(1) keV, respectively. From these results, the 2^+ energies are steeply decreasing in the Cr chain when approaching $N = 40$, which indicate that the Cr isotopes are strongly deformed. Shell model calculations need to take into account the intruder g and d orbitals in order to reproduce this trend. The combined effects of the $N = 40$ shell gap breaking and the $d_{5/2}$ lowering bring a sequence of levels j, $j-2$ above the Fermi surface which favors quadrupole $E2$ excitations in the neutron-rich Cr isotopes. This consequently explains the onset of quadrupole deformation in the ^{62}Cr region.

F. N. and A. P. would like to thank M. Hjorth-Jensen for making available to us his Two-Body realistic Matrix elements.

References

1. J. Dobaczewski, I. Hamamoto, W. Nazarewicz, J.A. Sheikh, Phys. Rev. Lett. **72**, 981 (1994).
2. O. Sorlin *et al.*, Phys. Rev. Lett. **88**, 092501 (2002).
3. M. Hannawald *et al.*, Phys. Rev. Lett. **82**, 1391 (1999).
4. O. Sorlin *et al.*, Nucl. Phys. A **669**, 351 (2000).
5. L. Weissman *et al.*, Phys. Rev. C **59**, 2004 (1999).
6. U. Bosch *et al.*, Nucl. Phys. A **477**, 89 (1988).
7. S. Franchoo *et al.*, Phys. Rev. C **64**, 054308 (2001).
8. W.F. Mueller *et al.*, Phys. Rev. Lett. **83**, 3613 (1999).
9. J.I. Prisciandaro *et al.*, Phys. Rev. C **60**, 054307 (1999).
10. E. Runte *et al.*, Nucl. Phys. A **399**, 163 (1983).
11. P. Möller, J.R. Nix, K.-L. Kratz, At. Data Nucl. Data Tables **66**, 131 (1997).
12. J.M. Daugas, PhD Thesis (1999), Université de Caen, GANIL-T 9905.
13. P. Möller, J. Randrup, Nucl. Phys. A **514**, 1 (1990).
14. H.L. Seifert *et al.*, Z. Phys. A **349**, 25 (1994).
15. S. Raman *et al.*, Phys. Rev. C **37**, 805 (1988).
16. S. Raman *et al.*, Phys. Rev. C **43**, 556 (1991).
17. J.I. Prisciandaro *et al.*, Phys. Lett. B **510**, 17 (2001).
18. S. Raman *et al.*, At. Data. Nucl. Data. Tables **36**, 1 (1987).
19. Y. Aboussir *et al.*, At. Data Nucl. Data Tables **61**, 127 (1995).
20. S. Leenhardt *et al.*, Eur. Phys. J. A **14**, 1 (2002).
21. H. Grawe *et al.*, *Tours Symposium on Nuclear Physics IV, Tours 2000*, AIP Conf. Proc. **561**, 287 (2001).
22. A. Huck *et al.*, Phys. Rev. C **31**, 2226 (1985).
23. R. Kanungo, I. Tanihata, A. Ozawa, Phys. Lett. B **528**, 58 (2002).
24. O. Sorlin *et al.*, Nucl. Phys. A **632**, 205 (1998).
25. A. Poves, J. Sanchez Solano, E. Caurier, F. Nowacki, Nucl. Phys. A **694**, 157 (2001).
26. W.A. Richter, M.G. van der Merwe, R.E. Julies, B.A. Brown, Nucl. Phys. A **523**, 325 (2001).
27. R. Grzywacz *et al.*, Phys. Rev. Lett. **81**, 766 (1998).
28. A.P. Zuker, J. Retamosa, A. Poves, E. Caurier, Phys. Rev. C **52**, R1741 (1995).
29. E. Caurier *et al.*, in *ENAM2001*, Eur. Phys. J. A **15**, 145 (2002).
30. M. Hjorth-Jensen, T.T.S. Kuo, E. Osnes, Phys. Rep. **261**, 125 (1995); M. Hjorth-Jensen, private communication.
31. T. Otsuka, R. Fujimoto, Y. Utsuno, B.A. Brown, M. Honma, T. Mizusaki, Phys. Rev. Lett. **87**, 082502 (2001).
32. S. Hankonen, P. Baumann, E. Caurier, P. Dessagne, A. Jokinen, A. Knipper, C. Miehe, F. Nowacki, M. Oinonen, Z. Radivojevic, M. Ramdhane, G. Walter, J. Aysto, Phys. Rev. C **63**, 044316 (2001).
33. S. Hankonen, F. Nowacki, P. Baumann, E. Caurier, S. Courtin, P. Dessagne, A. Jokinen, A. Knipper, G. Le Scornet, L.G. Lyapin, C. Miehe, M. Oinonen, E. Poirier, Z. Radivojevic, M. Ramdhane, W.H. Trzaska, G. Walter, J. Aysto, Phys. Rev. C **64**, 054313 (2001).